ChemComm

COMMUNICATION

View Article Online
View Journal

Cite this: DOI: 10.1039/c9cc01601e

Received 26th February 2019,
Accepted 15th March 2019

DOI: 10.1039/c9cc01601e

rsc.li/chemcomm

A cucurbituril/polysaccharide/carbazole ternary supramolecular assembly for targeted cell imaging†

Xuan Wu,[a] Yong Chen,[ab] Qilin Yu,[c] Feng-Qing Li[a] and Yu Liu *[ab]

A carbazole derivative (G) was synthesized as a photosensitizer to complex with cucurbit[8]uril, resulting in a nanocube with emission at 662 nm for lysosome cell imaging. Furthermore, the alkyl chain on G was included by α-cyclodextrine-modified hyaluronic acid for further assembly, affording a system targeted to cancer cells.

Far-red and near-infrared (NIR) (650–1000 nm) dyes[1,2] have been extensively studied and explored as photosensitizers in the fields of cancer diagnosis and therapy, as they cause less photo-damage to cells, and have lower scattering, deeper light penetration, and better separation from the auto-fluorescence of the medium.[3–7] Traditionally, the synthesis of this type of dye is always complex and tedious, especially for dyes containing targeted motifs, or some other functional groups for combined therapy. Therefore, how to construct a versatile system in a convenient way remains a challenge. As an effective approach to constructing functional systems, supramolecular assembly has attracted tremendous attention.[8–11] In these systems, the building blocks are assembled into well-defined arrangements through non-covalent interactions to achieve versatile functions. Therefore, with careful design of the building blocks, we could fabricate a versatile assembly from simple molecules, thus enabling us to construct a system with both NIR imaging and targeted photodynamic therapy (PDT) properties in a relatively convenient way.

As is well known, cucurbit[8]uril[12] (**CB[8]**) has been widely studied for the construction of emission-tunable systems due to its ability to restrict the rotation of guest molecules, and form an extended conjugation system.[13–16] Therefore, with careful design of the guest molecules, a NIR emission system could be achieved by complexation between **CB[8]** and the non-NIR dye, which could be used as the first-stage assembly. Recently, Liu and coworkers reported a **CB[8]**-mediated NIR lysosome imaging system, in which the emission of the guest molecule (4,4′-anthracene-9,10-diylbis(ethene-2,1-diyl)bis(1-ethylpyridin-1-ium)bromide) could shift to the NIR region after complexation with **CB[8]**.[17] However, there was no other binding site for the introduction of the secondary functional motif. Following this line, we envisioned the addition of another binding site onto the guest molecule, which would enable further assembly for combined functions. To the best of our knowledge, few studied have focused on both **CB[8]**-based NIR imaging and targeted PDT systems. Based on previous studies, molecules with a strong intramolecular push–pull effect could lower the energy gap between the S_1 and T_1 states, which could benefit the intersystem crossing efficiency for the generation of singlet oxygen ($^1O_2$) or other reactive oxygen species (ROS).[18–21] Herein, a supramolecular system with NIR lysosome imaging and targeted PDT abilities has been constructed in a two-step assembly. Firstly, a dipolar fluorescence compound (**G**) with carbazole as the electron donor motif and pyridinium as the electron acceptor motif was synthesized, exhibiting an emission wavelength at 568 nm. After the formation of a supramolecular complex with **CB[8]**, the binary assembly could assemble into a nanocube with an average diameter of around 220 nm (Scheme 1). To our delight, the emission peak exhibited a remarkable shift to 662 nm. Besides, ROS generation was also improved about 1.5 times compared with **G**, and a cell assay certificated that this binary system could also be used as a lysosome imaging agent as well as a photosensitizer for cancer treatments. Moreover, due to the long alkyl chain on the **G**, α-cyclodextrine-modified hyaluronic acid (**HA-CD**) was introduced into the secondary assembly,[22,23] resulting in the formation of supramolecular nanoparticles without changing the emission wavelength and ROS generation ability. Therefore, a targeted PDT system could be constructed, which exhibited low light cytotoxicity to normal cells (293T), but high cytotoxicity to cancer cells (A549).

[a] College of Chemistry, State Key Laboratory of Elemento-Organic Chemistry, Nankai University, Tianjin, 300071, China. E-mail: yuliu@nankai.edu.cn
[b] Collaborative Innovation Center of Chemical Science and Engineering (Tianjin), Tianjin, 300071, China
[c] Department of Microbiology, College of Life Sciences, Nankai University, Tianjin, 300071, China

† Electronic supplementary information (ESI) available: Details of synthesis procedure, UV-vis and fluorescence spectra, DLS and zeta potential results, TEM and SEM images, and fluorescence images of cells. See DOI: 10.1039/c9cc01601e

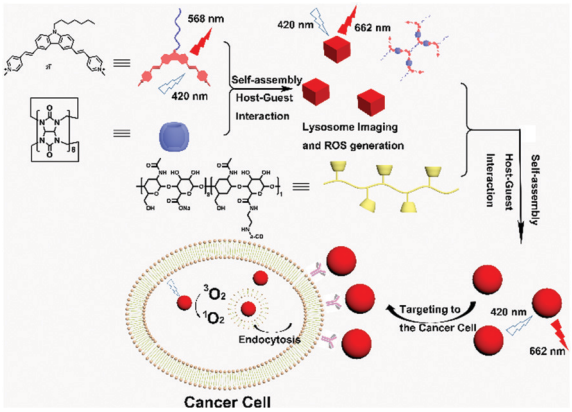

Scheme 1 Schematic illustration of the construction of the targeting PDT system.

Firstly, the host–guest properties between **G** and **CB[8]** were studied. Due to its poor solubility in aqueous solution, another similar compound (**MG**), with a shorter alkyl chain and different counterion, was successfully synthesized. As shown in Fig. 1, an upfield chemical shift and broadening effect of the protons H_{e-h} on **MG** were observed in the presence of **CB[8]**, as well as a downfield shift of the protons H_{b-d}, resulting from the inclusion of a pyridium motif in the cavity of **CB[8]**. Moreover, 2D NOESY spectroscopy also confirmed these results by the observation of strongly correlated signals between the protons H_c and H_f (Fig. S10, ESI†).

Furthermore, a Job's plot indicated the 1 : 1 binding stoichiometry between **CB[8]** and **G** (Fig. S11, ESI†). And the binding constant was determined to be $(3.38 \pm 0.23) \times 10^6$ M^{-1}. From the recorded spectra (Fig. S12, ESI†), an obvious red-shift in the absorption peak of **G** was observed upon the gradual addition of **CB[8]**, in which two isoabsorptive points were observed at 466 nm and 482 nm. The changes in the solution color also provided visible evidence for the above mentioned change, in which the color of the solution changed from yellow to red upon

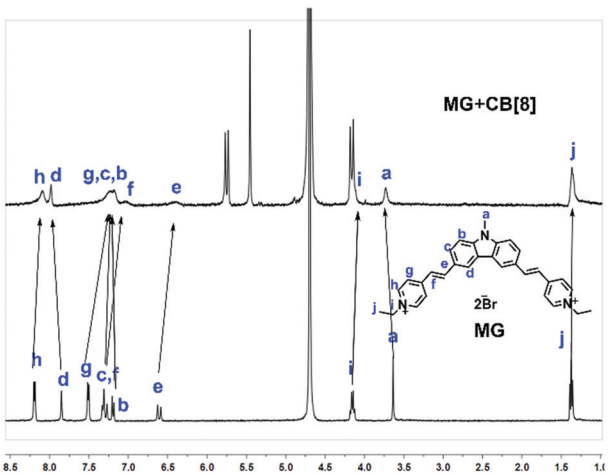

Fig. 1 Partial ^{1}H NMR spectra (400M Hz, 298 K, D_2O) of (a) **MG** ([**MG**] = 2 mM), and (b) **MG** + **CB[8]** ([**MG**] = [**CB[8]**] = 2 mM).

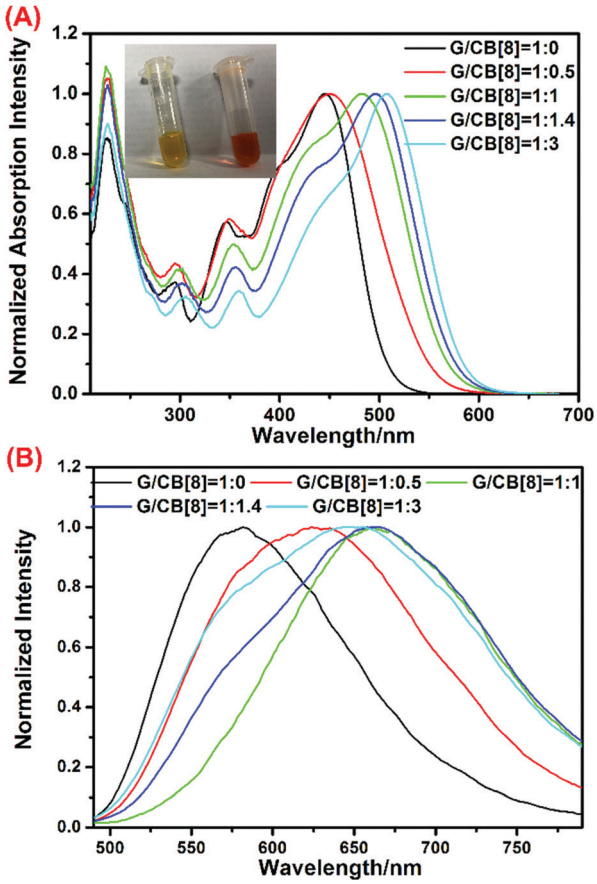

Fig. 2 (a) Normalized UV-vis spectra of **G** with various molar ratios of **CB[8]** ([**G**] = 2×10^{-4} M), and (b) normalized fluorescence spectra of **G** with various molar ratios of **CB[8]** ([**G**] = 2×10^{-5} M). Insets in panel (a) are photos of the **G** solution before and after the addition of **CB[8]**.

the gradual addition of **CB[8]** (Fig. 2a, inset). The occurrence of two isoabsorptive points during the UV-vis titration attracted our attention. Therefore, a 2D diffusion-ordered ^{1}H NMR spectroscopy (DOSY) experiment was performed, and the diffusion coefficient of low concentration (2 mM) was recorded. From the DOSY spectrum (Fig. S13, ESI†), only one set of signals could be observed. And the radius in D_2O was calculated to be 1.55 nm by the Stokes–Einstein relationship (Table S1, ESI†), and the molecular size of **MG** was about 1.35 nm (Fig. S14, ESI†). Therefore, there might exist stable oligomers at a molar ratio of 1 : 1 between **CB[8]** and **G**. And the continual addition of **CB[8]** could destroy the oligomers, thus resulting in the formation of the second isoabsorptive point, which was consistent with the UV-vis titration experiment.

Fluorescence spectroscopy was also carried out to determine the red-shift of **G** after formation of complexation with **CB[8]**. As shown in Fig. 2b, the maximum emission wavelength of **G** was at 568 nm with a weak emission band, and the fluorescence quantum yield was determined to be 0.69%, while the fluorescence lifetime was 0.60 ns (Fig. S15a, ESI†). After complexation with **CB[8]** at a molar ratio of 1 : 1 ([**G**]/[**CB[8]**]), the maximum emission wavelength exhibited a remarkable red-shift to 662 nm in the NIR region (Fig. 2b), and the fluorescence quantum yield

was 2.14%, and the lifetime was 4.21 ns (Fig. S15b, ESI†). Through continually adding **CB[8]** at a molar ratio of 1 : 1.4 ([**G**]/[**CB[8]**]), a new emission peak appeared at 568 nm, indicating the destruction of the previous assembly. However, if the molar ratio between [**G**] and [**CB[8]**] was 1 : 3, the emission peak would exhibit a blue shift as well as the increased intensity at 568 nm. This result could also prove the formation of a stable oligomer at a molar ratio of 1 : 1 ([**CB[8]**]/[**G**]), but the continual addition of **CB[8]** would destroy the formed oligomer.

Due to the amphipathy of **G**, the self-assembly morphologies in the presence and absence of **CB[8]** were investigated. From the TEM and SEM images (Fig. 3a and c), **G** could self-assemble into nanofibers in aqueous solution. Meanwhile the **G⊂CB[8]** complexation could self-assemble into nanocubes (Fig. 3b and d) with a broad diameter distribution ranging from 200–600 nm, and the average diameter was determined to be around 220 nm by DLS analysis (Fig. S16b, ESI†). Moreover, the obtained nanocube had a positively charged surface, the value of which was measured to be +49.6 mV (Fig. S17b, ESI†). Moreover, their ROS and $^1O_2$ generation abilities were studied using commercially available probes (details in Fig. S18, ESI†), and both the ROS and $^1O_2$ generation abilities were enhanced after the addition of **CB[8]**, indicating their potential application in PDT. Based on the above results, it was concluded that the NIR emission assembly with enhanced PDT efficiency was simply constructed by the host–guest interactions between **CB[8]** and **G**.

To examine the biological applications of the obtained supramolecular assembly, a cell imaging experiment was carried out. After being incubated with **G⊂CB[8]** solution followed by observation under a laser scanning confocal microscope, bright green fluorescence within A549 cells (purchased from Cell Center of Peking Union Medical College Hospital, China) can be observed in the dye channel. A further colocalization experiment by co-incubating with LysoTracker (purchased from Invitrogen Co., Ltd, USA) indicated that the formed nanoparticles could stain lysosome specifically (Fig. S19, ESI†). Then the standard 3-(4,5-dimethylthiazol-2-yl)-2,5-diphenyltetrazolium bromide (MTT, purchased from Amresco Co., Ltd, USA) assay was carried out to evaluate the anti-cancer abilities. The A549 cancer cells were incubated with **G**, **CB[8]** and **G⊂CB[8]** respectively, then their viability was calculated under different conditions. As shown in Fig. S20a (ESI†), less than 5% of A549 cells were killed in the dark environment. Even at a relatively high concentration, the cell viability was more than 95%, meaning relatively low cytotoxicity in dark conditions, and acceptable biocompatibility. Upon irradiation under white light, cell viability rapidly decreased. As illustrated in Fig. S20b (ESI†), 82% of cells were killed in the presence of **G⊂CB[8]** under light irradiation at a concentration of 2 μM ([**CB[8]**] = [**G**] = 2 μM), and almost no alive cells could be detected at a concentration of 4 μM. This phenomenon was consistent with the previous results that addition of **CB[8]** could improve the ROS generation ability. This result also confirmed that the NIR and enhanced PDT system was conveniently constructed through first-step assembly.

After successful construction of the binary assembly, **HA-CD** was introduced for further assembly, thanks to host–guest interactions with the alkyl chain and electrostatic interactions. Therefore, the obtained ternary system would be endowed with targeting properties for the cancer cells.[24,25] Firstly, a Job's plot indicated the 1 : 1 binding stoichiometry between α-CD and **G** (Fig. S21, ESI†), and the binding affinity was determined to be $(5.9 \pm 0.4) \times 10^3\ M^{-1}$ (Fig. S22, ESI†). Furthermore, a circular dichroism spectrum confirmed the inclusion of the alkyl chain into the cavity of α-CD (Fig. S24, ESI†). A similar phenomenon could also be observed in the process of UV-vis titration between α-CD and **G⊂CB[8]** (Fig. S23, ESI†), where only the absorption intensity decreased upon the gradual addition of α-CD, meaning the previous binding model could not be destroyed. This result provided a foundation for the construction of the targeted ternary system.

The **HA-CD** was successfully synthesized with a degree of substitution of 11%. The addition of **HA-CD** to **G⊂CB[8]** solution had no influence on its fluorescence emission and UV-vis absorption properties, as shown in Fig. S25 (ESI†). Subsequently, TEM and SEM images indicated that the ternary system could form nanoparticles with an average diameter of around 500 nm (Fig. S26 and S27a, ESI†) and a negative charge distribution (−18 mV) on the surface (Fig. S27b, ESI†), indicating the distribution of **HA-CD** on the surface, which would provide the obtained ternary system with targeting properties. Moreover, the ROS generation ability was also retained by using H2DCF-DA as a ROS indicator (Fig. S28, ESI†).

To our delight, the introduction of **HA-CD** could reduce the uptake of **HA-CD@G⊂CB[8]** into normal cells (293T, purchased from the Cell Center of Peking Union Medical College Hospital, China), as concluded from the fluorescence images of cells (Fig. S29, ESI†). Then the MTT assay was carried out to further evaluate the targeted efficiency. As shown in Fig. 4, **G⊂CB[8]** could induce cell death in half of the 293T cells even at a relatively low concentration; meanwhile, the addition of **HA-CD** could reduce the photo-damage to the normal cells, as more than 90% remained alive under the same conditions. What's more, this ternary system could also retain its phototoxicity to

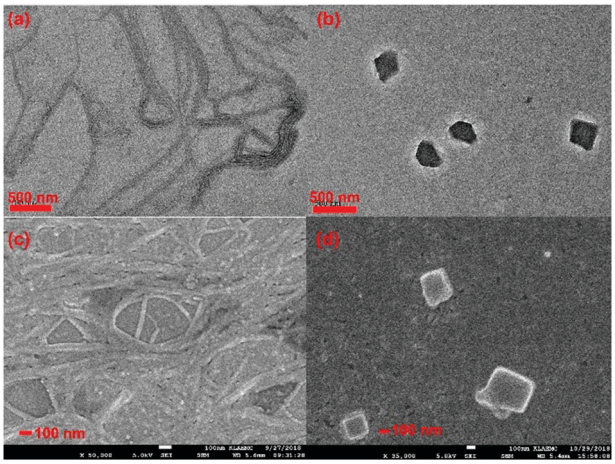

Fig. 3 (a) TEM image of **G**, (b) TEM image of **G⊂CB[8]**, (c) SEM image of **G**, and (d) SEM image of **G⊂CB[8]**.

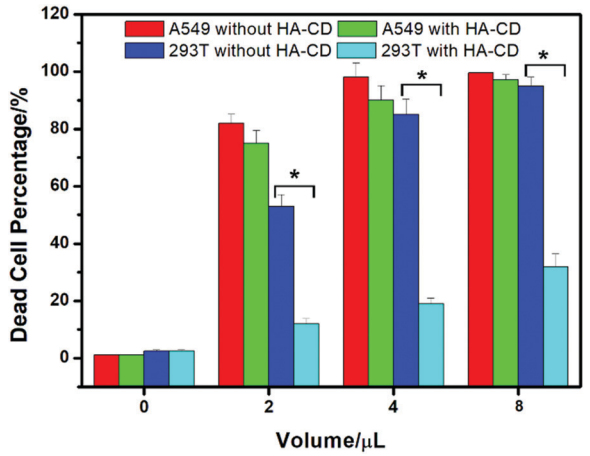

Fig. 4 The concentration dependent MTT assay of **HA-CD@G⊂CB[8]** and **G⊂CB[8]** with normal cells (293T) and cancer cells (different volumes of **HA-CD@G⊂CB[8]** and **G⊂CB[8]** solution were added into the cell solution (100 μL) and irradiated under white light, [**CB[8]**] = [**G**] = 1×10^{-4} M, [**HA-CD**] = 0.04 mg mL^{-1}) ($P < 0.05$, *).

cancer cells (A549). And these results confirmed the successful construction of a functional NIR imaging and targeted PDT system by multi-step assembly.

Herein, a ternary supramolecular assembly was successfully constructed using **G**, **CB[8]** and **HA-CD** with a multi-step assembly method, and could be used as a targeted NIR lysosome probe and PDT agent. Firstly, a carbazole derivative (**G**) with multi binding sites was synthesized as the photosensitizer, and was a non-NIR emission dye with the emission wavelength at 568 nm. After the formation of a host–guest complexation with **CB[8]**, its fluorescence spectrum exhibited a remarkable red shift to 662 nm. Moreover, this binary assembly could be used for targeted NIR lysosome imaging and act as an efficient PDT agent. Finally, **HA-CD** was incorporated into the secondary assembly, due to the strong host–guest interactions between the alkyl chain and α-CD, which afforded a ternary nano-supramolecular assembly with targeting properties. Due to the overexpressed acceptors on cancer cell surfaces, this ternary assembly could remarkably reduce the light cytotoxicity of the **G⊂CB[8]** complex to normal cells (293T), while retaining light cytotoxicity to cancer cells (A549). Therefore, taking advantage of orthogonal host–guest recognition with different macrocyclic molecules, a complex system with an ability for NIR imaging and enhanced targeted PDT efficiency was successfully constructed in a relatively convenient way, which would provide a new strategy for the construction of efficient cancer diagnosis and therapy systems by careful design of the basic building blocks.

We thank the National Natural Science Foundation of China (grant no. 21672113, 21432004, 21772099, 21861132001 and 91527301) for financial support.

Conflicts of interest

There are no conflicts to declare.

Notes and references

1 R. Kumar, W. S. Shin, K. Sunwoo, W. Y. Kim, S. Koo, S. Bhuniya and J. S. Kim, *Chem. Soc. Rev.*, 2015, **44**, 6670.
2 M. Gao, F. Yu, C. Lv, J. Choo and L. Chen, *Chem. Soc. Rev.*, 2017, **46**, 2237.
3 A. P. Castano, P. Mroz and M. R. Hamblin, *Nat. Rev. Cancer*, 2006, **6**, 535.
4 J. P. Celli, B. Q. Spring, I. Rizvi, C. L. Evans, K. S. Samkoe, S. Verma, B. W. Pogue and T. Hasan, *Chem. Rev.*, 2010, **110**, 2795.
5 A. Kamkaew, S. H. Lim, H. B. Lee, L. V. Kiew, L. Y. Chung and K. Burgess, *Chem. Soc. Rev.*, 2013, **42**, 77.
6 C. Mari, V. Pierroz, S. Ferrari and G. Gasser, *Chem. Sci.*, 2015, **6**, 2660.
7 N. Mehwish, X. Dou, Y. Zhao and C.-L. Feng, *Mater. Horiz.*, 2019, **6**, 14.
8 Q. Yu, Y.-M. Zhang, Y.-H. Liu, X. Xu and Y. Liu, *Sci. Adv.*, 2018, **4**, 2297.
9 S.-H. Li, H.-Y. Zhang, X. Xu and Y. Liu, *Nat. Commun.*, 2015, **6**, 7590.
10 X. Wu, L. Gao, X.-Y. Hu and L. Wang, *Chem. Rec.*, 2016, **16**, 1216.
11 S. Guo, Y. Song, Y. He, X.-Y. Hu and L. Wang, *Angew. Chem., Int. Ed.*, 2018, **57**, 3163.
12 S. J. Barrow, S. Kasera, M. J. Rowland, J. del Barrio and O. A. Scherman, *Chem. Rev.*, 2015, **115**, 12320.
13 S.-H. Li, X. Xu, Y. Zhou, Q. Zhao and Y. Liu, *Org. Lett.*, 2017, **19**, 6650.
14 X. Tang, Z. Huang, H. Chen, Y. Kang, J.-F. Xu and X. Zhang, *Angew. Chem., Int. Ed.*, 2018, **57**, 8545.
15 X.-L. Ni, S. Chen, Y. Yang and Z. Tao, *J. Am. Chem. Soc.*, 2016, **138**, 6177.
16 Y. Kang, X. Tang, H. Yu, Z. Cai, Z. Huang, D. Wang, J.-F. Xu and X. Zhang, *Chem. Sci.*, 2017, **8**, 8357.
17 X.-M. Chen, Y. Chen, Q. Yu, B.-H. Gu and Y. Liu, *Angew. Chem., Int. Ed.*, 2018, **57**, 12519.
18 S. Liu, H. Zhang, Y. Li, J. Liu, L. Du, M. Chen, R. T. K. Kwok, J. W. Y. Lam, D. L. Phillips and B. Z. Tang, *Angew. Chem., Int. Ed.*, 2018, **57**, 15189.
19 D. Wang, M. M. S. Lee, G. Shan, R. T. K. Kwok, J. W. Y. Lam, H. Su, Y. Cai and B. Z. Tang, *Adv. Mater.*, 2018, **30**, 1802105.
20 F. Hu, S. Xu and B. Liu, *Adv. Mater.*, 2018, **30**, 1801350.
21 Z. Zheng, T. Zhang, H. Liu, Y. Chen, R. T. K. Kwok, C. Ma, P. Zhang, H. H. Y. Sung, I. D. Williams, J. W. Y. Lam, K. S. Wong and B. Z. Tang, *ACS Nano*, 2018, **12**, 8145.
22 A. Hashidzume and A. Harada, *Polym. Chem.*, 2011, **2**, 2146.
23 Y. Takashima, K. Otani, Y. Kobayashi, H. Aramoto, M. Nakahata, H. Yamaguchi and A. Harada, *Macromolecules*, 2018, **51**, 6318.
24 Y. Yang, Y.-M. Zhang, Y. Chen, J.-T. Chen and Y. Liu, *J. Med. Chem.*, 2013, **56**, 9725.
25 Y. Yang, Y.-M. Zhang, Y. Chen, D. Zhao, J.-T. Chen and Y. Liu, *Chem. – Eur. J*, 2012, **18**, 4208.